Soils and Foundations 2015;55(2):315–328

HOSTED BY

ELSEVIER

CrossMark

The Japanese Geotechnical Society

Soils and Foundations

www.sciencedirect.com
journal homepage: www.elsevier.com/locate/sandf

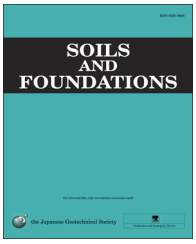

Axial capacity degradation of single piles in soft clay under cyclic loading

Maosong Huang[a,b,*], Ying Liu[a,b,c]

[a]Department of Geotechnical Engineering, Tongji University, Shanghai 200092, China
[b]Key Laboratory of Geotechnical and Underground Engineering of Ministry of Education, Tongji University, Shanghai 200092, China
[c]College of Civil Engineering and Architecture, Guangxi University, Nanning, 530004 China

Received 27 December 2013; received in revised form 3 November 2014; accepted 19 November 2014
Available online 20 March 2015

Abstract

A kinematic hardening constitutive model with von Mises failure criterion considering cyclic degradation was developed to analyze the cyclic axial response of single piles in saturated clay. After validation by comparison against published triaxial test results, this model was applied to a numerical simulation developed for computing the axial bearing capacity of a pile foundation subjected to a cyclic loading. The axial bearing capacity degradation of a single pile under different cyclic load levels and different cyclic load numbers was studied. It was found that the pile–soil system remains elastic at very low cyclic load levels, and the degradation of pile capacity happens when the cyclic load level increases. A higher cyclic load level after more cycles leads to faster degradation. In order to improve the computational efficiency, a simplified analysis method based on a simple nonlinear soil model is presented for the cyclic axial capacity degradation of single piles. The results calculated by this simplified analysis are consistent with those of the numerical simulation. Comparisons with laboratory test data suggest that both the finite element method and the simplified analysis method provide reasonable estimates of the axial pile capacity degradation of a single pile after cyclic loading.

Keywords: Kinematic hardening; Cyclic degradation; Axial pile capacity; Simplified analysis method

1. Introduction

Pile foundations are the predominant foundation concept for offshore wind turbines at present in moderate water depths up to 20–30 m (Lesny and Hinz, 2009). Although pile foundations are relatively simple and involve a straightforward design, their behavior is complex, subject to a variety of load conditions, all of which have to be considered. In a marine environment, besides the work load of wind turbine, environmental loads such as wind, waves and currents can cause long term axial and lateral cyclic loads to the pile foundation, which unavoidably have some detrimental effects. The degradation of pile stiffness and capacity, in particular, is potentially hazardous to the safety of the wind turbine structure. Although the lateral response of piles under cyclic loading is important for the design of offshore wind turbine foundations, the axial response still requires further attention.

Many researchers have investigated the axial response of piles in clay subjected to cyclic axial loads. A theoretical analysis published by Poulos (1979) was the first outline of an effective stress approach based on elastic theory, in which excess pore pressure is caused by cyclic loading in the soil adjacent to the pile, and soil stiffness and skin resistance are consequently reduced. An improved method later developed to consider the total stress (Poulos, 1981) can be applicable to a

*Corresponding author at: Department of Geotechnical Engineering, Tongji University, 1239 Siping Road, Shanghai 200092, China. Tel./fax: +86 21 65983980.
E-mail address: mshuang@tongji.edu.cn (M. Huang).
Peer review under responsibility of The Japanese Geotechnical Society.

http://dx.doi.org/10.1016/j.sandf.2015.02.008

wide range of problems. A cyclic stability diagram was then suggested with the mean and cyclic axial loads on a pile plotted and the three regions identified: the stable zone, the metastable zone and the unstable zone (Poulos, 1988). Lee (1993) presented a simplified cycle-by-cycle total stress hybrid load-transfer approach for analyzing the behavior of pile groups in clay under cyclic axial loading. In their work, degradation factors, empirically expressed as functions of the number of loading cycles were introduced.

Based on experimental tests carried out at normal gravity, Poulos (1979) found failure during cyclic loading occurred in several tests at a cyclic load level, P_c/P_{us}, between 0.56 and 0.62, and the number of cycles to failure ranging between 13 and 64. The cyclic degradation of the toe resistance for piles was indicated to be less significant than the cyclic degradation of shaft resistance (Poulos, 1987). Jardine and Standing (2012) found that two-way conditions may promote more severe cyclic losses than a one-way condition to the axial capacity of piles at the same cyclic loading level in full-scale field tests. Different patterns of the development of effective stress were reported in the experiments involving a highly instrumented model displacement pile and an array of soil stress sensors (Tsuha et al., 2012). These observations of the stress–strain behavior of the soil made a good understanding of three styles (stable, metastable and unstable) of pile responses under different cyclic loading levels. Lombardi et al. (2013) conducted a series of 1 g model tests to investigate the external dynamic and cyclic loading acting on a typical offshore wind turbine in soft saturated clay. A zone of soil softening around the pile was found after cyclic loading, and the increased moisture content of nearby clay evidently implies a reduction in the undrained strength and a decrease in the stiffness of the clay. The results of these experimental studies can be used for comparisons with theoretical predictions.

To gain a better understanding of the interaction of structure and soil under cyclic loading, the behavior of clays under cyclic loading must be considered. According to previous experimental studies, the modulus of saturated soft clays is degraded during cyclic loading and the undrained shear strength is reduced after cyclic loading. Factors such as the overconsolidation ratio, the confining pressure and the cyclic stress level have been examined in detail, and many empirical formulas have been set up (Sangrey et al., 1969; Andersen et al., 1980; Hyodo et al., 1994; Zergoun and Vaid, 1994; Soroush and Soltani-Jigheh, 2009; Huang and Li, 2010). However, according to the literature, these empirical formulas are seldom applied in practice to analyze the interaction of the structure and soil under cyclic loading.

Elasto-plastic models for clays in terms of total stress are usually chosen for the analysis of the cyclic response of a single pile because of their simplicity. Because the dissipation of pore water pressure is not considered in these models, the analysis results are relatively conservative. The constitutive models can be broadly divided into two categories. The models in the first category describe the dynamic stress–strain curve for soils directly by mathematical formulas, and are represented by the Hardin and Drnevich (1972) hyperbolic model and Ramberg and Osgood (1943) model. Models in the second category are based on the elasto-plastic theory and calculate the stress and strain relationship by certain yield criteria and hardening rules; examples are the kinematic hardening models and bounding surface models (Prévost, 1977; Mróz et al., 1981; etc.). While the models in the second category are more rigorous in theory, a number of the parameters needed may be difficult to determine, leading to further complicated numerical requirements. To date, a simplified kinematic hardening constitutive model with the von Mises failure criterion developed in the commercial finite element software ABAQUS has been used for the analysis of the cyclic response of shallow and deep foundations (Anastasopoulos et al., 2011; Giannakos et al., 2012).

The objective of this paper is to investigate the axial capacity degradation of single piles under cyclic loading in clay. At first, the simple kinematic hardening constitutive model in ABAQUS is modified slightly to describe the degradation behavior of clay under cyclic loading. Then this model is applied for calculating the axial bearing capacity of the pile in the FE analysis. Since the cyclic loading may recur millions of times in the entire service life of the structure, the computational efficiency must be improved to make it possible to carry out long-term loading calculations for engineering applications. Hence, a simplified analysis procedure based on a simple nonlinear model which considers cyclic degradation for the axial capacity degradation of the single pile under cyclic loading is presented in the last part of this paper. The proposed simplified method is validated by comparing with the FE analysis of the simplified kinematic hardening model and the model test results in the literature.

2. A kinematic hardening constitutive model considering cyclic degradation

2.1. Basic model description

The model presented herein is modified from a kinematic hardening model with von Mises failure criterion, which is available in ABAQUS. The model was developed originally based on the work of Armstrong and Frederick (1966) and Lemaitre and Chaboche (1990). This model can be used for the total stress analysis of clayey soils under undrained conditions. In what follows, a brief introduction of the basic model available in ABAQUS is presented.

The total strain rate $\dot{\varepsilon}_{ij}$ is written in terms of the elastic and plastic strain rates $\dot{\varepsilon}^e_{ij}$ and $\dot{\varepsilon}^p_{ij}$ as

$$\dot{\varepsilon}_{ij} = \dot{\varepsilon}^e_{ij} + \dot{\varepsilon}^p_{ij} \tag{1}$$

The elastic behavior is modeled as linear elastic, and the yield surface is defined by the function

$$F = f(\sigma_{ij} - \alpha_{ij}) - A = 0 \tag{2}$$

where σ_{ij} is the stress tensor, A is the size of yield surface. α_{ij} is the backstress tensor, which determines the kinematic evolution of the yield surface in the stress space. $f(\sigma_{ij} - \alpha_{ij})$ is the

equivalent Mises stress with respect to the back stress α_{ij}, and can be defined as

$$f(\sigma_{ij}-\alpha_{ij})=\sqrt{\frac{3}{2}\left(s_{ij}-\alpha_{ij}^{dev}\right):\left(s_{ij}-\alpha_{ij}^{dev}\right)} \tag{3}$$

where s_{ij} is deviatoric stress tensor, and α_{ij}^{dev} is the deviatoric tensor of α_{ij}. During undrained loading, the yielding of clays is independent of the imposed octahedral normal total stress component $p=\sigma_{ii}/3$, only deviatoric stresses $s_{ij}=\sigma_{ij}-1/3\delta_{ij}(\sigma_{kk})$ need appear in the yield functions, thus von Mises yield surface can be used (Prévost, 1977).

Given the associated plastic flow, the plastic flow rate is

$$\dot{\varepsilon}_{ij}^{p}=\dot{\varepsilon}_{eff}^{p}\frac{\partial f(\sigma_{ij}-\alpha_{ij})}{\partial\sigma_{ij}} \tag{4}$$

where $\dot{\varepsilon}_{ij}^{p}$ is the rate of plastic strain, $\dot{\varepsilon}_{eff}^{p}$ is the equivalent plastic strain rate, $\dot{\varepsilon}_{eff}^{p}=\left((2/3)\dot{\varepsilon}_{ij}^{p}\dot{\varepsilon}_{ij}^{p}\right)^{1/2}$.

The evolution of the kinematic component of the yield stress is described by the expression

$$\dot{\alpha}_{ij}=\frac{C\dot{\varepsilon}_{eff}^{p}}{A}(\sigma_{ij}-\alpha_{ij})-\gamma\alpha_{ij}\dot{\varepsilon}_{eff}^{p} \tag{5}$$

where C is the initial kinematic hardening moduli, which is usually chosen as Young's modulus E, and γ is the nonlinear parameter, determine the rate at which the kinematic hardening moduli decrease with increasing plastic deformation. When ε_{eff}^{p} tends to infinity, the extreme value of backstress α_{ij} equals α^{s}, where $\alpha^{s}=C/\gamma$. Hence, the maximum yield stress can reach $A+\alpha^{s}$.

2.2. Consideration of undrained cyclic degradation

The kinematic hardening model can be conveniently used to model the undrained cyclic behavior of clayey soils. However, phenomena such as pore-pressure buildup and dissipation cannot possibly be captured. The model should be modified to be applicable for the undrained behavior of clay under cyclic loading.

It is found from the cyclic triaxial tests that the post-cyclic undrained shear strength and stiffness of the clays are reduced (Zergoun and Vaid, 1994; Soroush and Soltani-Jigheh, 2009; Huang and Li, 2010). Hence, a degradation model for the undrained shear strength and stiffness under cyclic loading is introduced into the basic constitutive model, which is the function of accumulative equivalent plastic strain $\varepsilon_{eff,c}^{p}$ ($\varepsilon_{eff,c}^{p}=\int\dot{\varepsilon}_{eff,c}^{p}dt$) induced by cyclic loading, given by

$$\delta=\delta_{res}+(1-\delta_{res})e^{-b\varepsilon_{eff,c}^{p}} \tag{6}$$

where b is a material parameter, reflecting the rate of degradation with accumulative strain due to the generation of excess pore pressure and structural damage during cyclic loading. The degraded strength ratio δ is defined as $\delta=S_u/S_{u\,\max}=q_u/q_{u\,\max}$, and residual strength ratio δ_{res} is defined as $\delta_{res}=S_{ures}/S_{u\,\max}=q_{ures}/q_{u\,\max}$.

Eq. (6) can be rewritten into

$$S_u=S_{u\,\max}+(S_{ures}-S_{u\,\max})\left(1-e^{-b\varepsilon_{eff,c}^{p}}\right) \tag{7}$$

where $S_{u\,\max}$ is the initial undrained shear strength of clay, S_u is the degraded undrained shear strength after cyclic loading, S_{ures} is the final residual undrained shear strength after cyclic loading, and q is the generalized shear stress defined as $q=\sqrt{3/2s_{ij}s_{ij}}$. For undrained triaxial tests, $q_u=2S_u$; and for general boundary-value problems, $q_u=\sqrt{3}S_u$.

In order to model the strength reduction, the yield surface is defined to shrink with the increase of accumulative equivalent plastic strain $\varepsilon_{eff,c}^{p}$ induced by cyclic loading. The size of yield surface A can be chosen as a function of accumulative equivalent plastic strain $\varepsilon_{eff,c}^{p}$

$$A=A_0+Q(1-e^{-b\varepsilon_{eff,c}^{p}}) \tag{8}$$

where A_0 is the yield stress at zero plastic strain, Q and b are the material parameters. According to Eqs. (6) and (7), Q in Eq. (8) is negative and determines the final minimum value of the yield surface size, which is A_0+Q when $\varepsilon_{eff,c}^{p}$ tends to infinity.

However, it is worth pointing out that this shrinkage of yield surface does not occur immediately after the generation of plastic strain. According to Carter et al. (1982), even though the form of the yield surface remains unchanged, its size is reduced in an isotopic manner if elastic unloading occurs. This characteristic of the model could efficiently avoid stress softening when resisting monotonic loads, so the initial maximum yield stress before cyclic loading can be determined definitely. This complement also can be implemented in ABAQUS through the simple user subroutine.

From the above, the initial maximum yield stress and the residual yield stress can be determined by $q_{u\,\max}=A_0+\alpha^{s}$ and $q_{ures}=A_0+Q+\alpha^{s}$. As a result, the degradation of the undrained shear strength has been realized by the combination of the kinematic hardening component and isotropic hardening component, i.e. Eq. (7) can be retrieved by combining $q_{u\,\max}$, q_{ures} and Eq. (8).

The stiffness degradation law for clayey soils obtained from cyclic triaxial test results can also be encoded in the user subroutine. According to results obtained by cyclic triaxial tests with bender element measurements (Huang and Li, 2010), the degradation law of stiffness for saturated Shanghai soft clay is similar to the strength of the soil. Thus, in the absence of relevant test data, stiffness degradation can simply be assumed to follow the same law as strength, which is $E=\delta E_0$, where E is Young's modulus and E_0 is the initial Young's modulus of clays.

Fig. 1 shows the stress-equivalent plastic strain relations of this proposed constitutive model, and the key stresses of this proposed model in π plane, in which q_d is the amplitude of cyclic deviatoric stress. Since the size of the yield surface remains unchanged under monotonic loading, the maximum stress $q_{u\,\max}$ is reached with the development of nonlinear kinematic hardening. If, however, elastic unloading occurs (in cyclic loading), the yield surface shrinks with the increase in equivalent plastic strain $\varepsilon_{eff,c}^{p}$. When monotonic loading is applied after cyclic loading, the yield stress degrades to q_u. If $\varepsilon_{eff,c}^{p}$ keeps increasing during cyclic loading, the yield surface tends toward its minimum size, which is A_0+Q, and

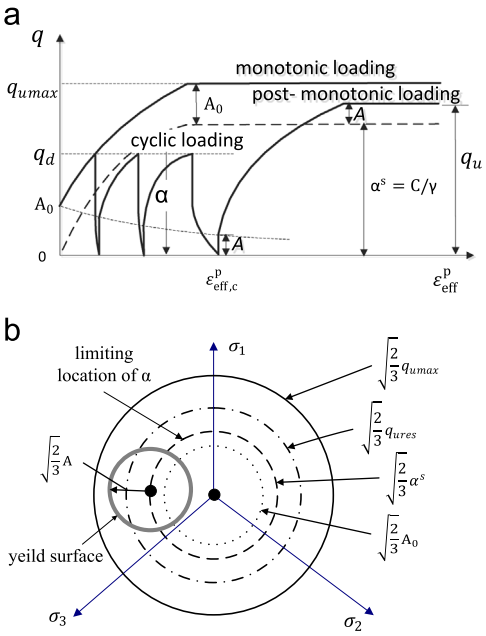

Fig. 1. Scheme of the kinematic hardening model: (a) stress-equivalent plastic strain relations; (b) three-dimensional representation of the key stresses.

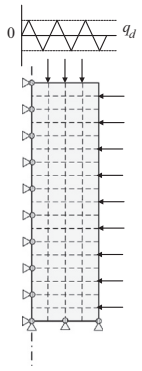

Fig. 2. Finite element model of dynamic triaxial tests.

Table 1
Parameters of saturated soft soil triaxial specimen in abaqus.

Elastic modulus	Poisson's ratio	Plastic modulus	Initial yield stress	Nonlinear parameter	Material parameter	Damping factor
E (kPa)	ν	C (kPa)	A_0 (kPa)	γ	Q (kPa)	b
300	0.49	300	2	30	−2	2

the yield stress degrades to its residual value q_{ures}. As shown in Fig. 1 (b), the center of the yield surface is contained within a cylinder of radius $\sqrt{2/3}\alpha^s$, and the yield surface is contained within the limiting surface of radius $\sqrt{2/3}q_{u\,\max}$. When considering the degradation of soil strength, this limiting surface will shrink to a radius of $\sqrt{2/3}q_{ures}$.

When the isotropic consolidated saturated clay is resisting undrained cyclic load with different amplitude values of q_d, three kinds of state will form. If $q_d \le A_0$, the soil is in elastic state, and degradation does not occur. If $A_0 < q_d \le q_{ures}$, the soil remains in an elastoplastic state, degradation occurs and a nonfailure equilibrium is reached. When $q_{ures} < q_d \le q_{u\,\max}$, the soil remains in an elastoplastic state, degradation occurs, and failure occurs as the number of cycles increases. However, with dynamic stress $q_d > q_{u\,\max}$, failure occurs at the first loading. In this aspect, the model is capable of describing the experimental phenomena in the literature reasonably well.

2.3. Model verification

A saturated clay triaxial specimen model is set up in ABAQUS (Fig. 2). The initial undrained shear strength of clay S_{u0} is fixed at 6 kPa and $\delta_{res} = 0.83$. Then the calculated values $q_{u\,\max} = 12$ kPa and $q_{ures} = 10$ kPa. Parameter A_0, which controls the initiation of the nonlinear behavior and determines the maximum degraded value from the initial yield stress $q_{u\,\max}$, typically ranging from $0.1q_{u\,\max}$ to $0.3q_{u\,\max}$, is chosen as 2 kPa. The degradation of soil stiffness is assumed to follow the same law as strength. The other parameters required by the model were calculated and are shown in Table 1. At first, a confining pressure of 20 kPa is applied to simulate the isotropic consolidation of clay. Then two-way (compression and tension) axial cyclic loading with a constant amplitude of q_d is applied for twenty cycles. Three representative amplitudes of deviatoric stress q_d 2 kPa, 6 kPa and 10.1 kPa are chosen for comparison. The stress–strain curves are presented in Fig. 3.

When the amplitude of deviatoric stress $q_d = 2$ kPa $\le A_0$, the soil is elastic, and the stress–strain hysteresis loops are just straight lines (Fig. 3a). When $A_0 < q_d = 6$ kPa $\le q_{ures}$, the soil is elastic–plastic, and plastic deformation accumulates gradually and degradation occurs. The stress–strain hysteresis loop becomes bigger, and closed stress–strain hysteresis loops are formed at last, indicating that a non-failure equilibrium is reached (Fig. 3b). When $q_{ures} < q_d = 10.1$ kPa $\le q_{u\,\max}$, plastic deformation accumulates remarkably quickly and the hysteresis loop becomes larger, with failure occurring at the fifth cycle (Fig. 3(c)).

To examine the efficiency of this model, the experimental results obtained by Sangrey et al. (1969) in their investigation of one-way cyclic loading on saturated clay were simulated. In their typical test, the specimens of saturated clay soil were subjected to a series of one-way cyclic loadings until either the specimen failed or a condition of nonfailure equilibrium was reached. Fig. 4 shows an overall picture of the relationship between deformation and the stress level obtained in the tests. The results of the monotonic loading test are shown in the upper curve, while the lower curve shows the axial strains associated with the stress peaks of the equilibrium hysteresis loops. Thus $q_{u\,\max} = 380$ kPa and $q_{ures} = 247$ kPa can be obtained from the two curves. To simulate the test results, A_0 is selected as 133 kPa, and the elastic modulus E is fixed at 40,000 kPa. However, there is no such a straightforward way to determine the value of material parameter b. It can

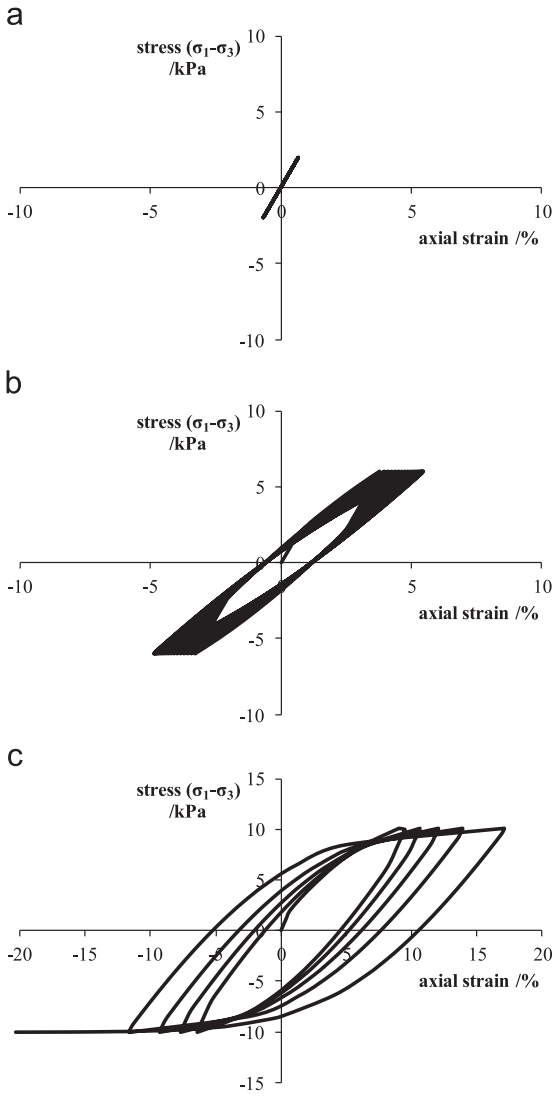

Fig. 3. Stress–strain hysteresis loops at different dynamic stresses.

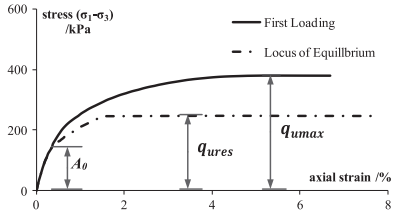

Fig. 4. Stress–strain behavior in the tests (Sangrey et al., 1969).

be back-figured from the stress–strain hysteresis loop of the test results (Fig. 6a). Assume that the failure of clay occurred after 10 cycles at the dynamic stress $q_d = 330$kPa, and the associated equivalent plastic strain ε^p_{eff} is selected to be approximately equal to the axial strain ($\varepsilon_1 = 12.3\%$). Considering the difference between the total strain and the plastic strain, parameter b was allocated a value of 3.2. The degradation of stiffness is assumed to follow the same law as strength in the absence of relevant test data.

The other parameters of the model are shown in Table 2. Comparisons between model simulations and test results can

Table 2
Parameters of the model for validation against triaxial tests.

Elastic modulus E (kPa)	Poisson's ratio ν	Plastic modulus C (kPa)	Initial yield stress A_0 (kPa)	Material parameter Q (kPa)	Nonlinear parameters γ
40,000	0.49	40,000	133	−133	162

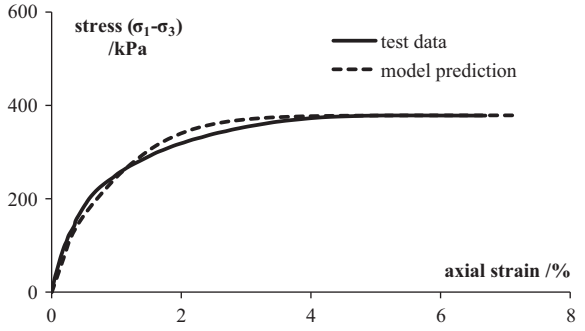

Fig. 5. Comparisons of stress–strain curves under monotonic loading.

be seen in Figs. 5 and 6. Stress–strain curves under monotonic loading and cyclic loading calculated from the model are in good agreement with test data. Since the degradation of the modulus of the soil is assumed as same as strength in the model, there is a little deviation on the development of hysteresis loops. However, the shape of subsequent stress–strain hysteresis loops remains the same from the second loop if degradation is not considered in this model, which is also shown in Fig. 6(b).

Despite the limitations mentioned above, the simplified kinematic hardening constitutive model needs only seven parameters. Earlier models (Prévost, 1977; Mróz et al., 1981) required more parameters, and the most encouraging is that the model can be conveniently applied in the complicated structure-soil system calculation with the help of commercially available finite element software.

3. Finite element simulations of axial capacity degradation of single piles

3.1. Parametric studies of a single pile under cyclic loading

The first numerical example is chosen to demonstrate the capacity of the proposed finite element procedure in simulating the response of a single pile under various cyclic load levels. A pile diameter of $D = 0.5$ m, a pile length of $L = 10$ m, an elasticity modulus of pile $E_p = 200$ GPa, and the Poisson's ratio $\nu_p = 0.2$ were used in the calculations. The following parameters were also assumed: the initial undrained shear strength of saturated soft clay $S_{u0} = 10$kPa, the elasticity modulus of soil $E_s = 300$ kPa, and the Poisson's ratio $\nu_s = 0.49$. Assume $\delta_{res} = 0.8$ and $b = 1$. The maximum of the yield stress $q_{u\,\max} = 17.3$ kPa, and the residual yield stress $q_{ures} = 13.8$ kPa. A_0 was chosen as $0.2q_{u\,\max}$, then $Q = -3.5$ kPa. The parameters used in this numerical example are shown in Table 3. The soil was assumed homogeneous.

The displacement-control mode and load-control mode are usually applied in cyclic loading analyses. Although computational convergence is easy to achieve in displacement-control analyses, a load-control analysis is closer to the actual situation and is more meaningful for engineering practice. Therefore, load-control analyses were performed in this study. After some certain cycles of the loading (No. of cycles = 10, 50, 100), a monotonic load was applied to find the ultimate bearing capacity (Q_{uc}), and Q_{us} is the ultimate bearing capacity without resisting cyclic load, Q_c is the amplitude of cyclic load. The values of cyclic load level Q_c/Q_{us} were selected as 0.1, 0.2, 0.3, 0.4, 0.6 and 0.8.

A 2D axisymmetric model is set up (Fig. 7). The calculated zone is 20 times the pile diameter in the horizontal plane, and twice the pile length, vertically. Eight-node second-order quadrilateral elements are applied in the meshing, with grid refinement adjacent to the pile. No relative displacement between the pile and soil was assumed. The bottom of the model was treated as a fixed boundary, while the vertical boundaries were constrained in the horizontal direction and rotated. Fig. 8 shows the load–displacement relations of the pile top at different cyclic load levels and Fig. 9 shows the stress–strain relations of soil around pile top. It can been observed than the shear stress levels of soil around pile top τ_c/S_{u0} are a little higher than the corresponding cyclic load levels Q_c/Q_{us} on the pile top. These curves become "fatter" with the increase in the cyclic load level. Both the force–displacement curve and stress–strain curve were straight lines at $Q_c/Q_{us} = 0.1$, revealing the pile–soil system remained elastic at small cyclic load levels during 100 cycles, without the occurrence of any degradation. As the cyclic load level gets greater, the cyclic displacement increases with the number of cycles increases, and the stress–strain loops lean gradually to the strain coordinate at the same time, which illustrates the degradation of the ultimate axial capacity and the stiffness of pile foundation during the cyclic loading, as well as the degradation of the strength and modulus of the soil around the pile. When the cyclic load level is large enough, failure occurs during cyclic loading. For example, when $Q_c/Q_{us} = 0.8$, failure occurs at the eighth cycle.

The ultimate bearing capacity after different number of cycles and different cyclic load levels are shown in Fig. 10. The degradation develops slowly with the increase of cyclic load level after fewer cycles (10 cycles), and the pace quickens after more cycles (50 cycles, 100 cycles). Under low cyclic loads, little or no degradation of the ultimate bearing capacity

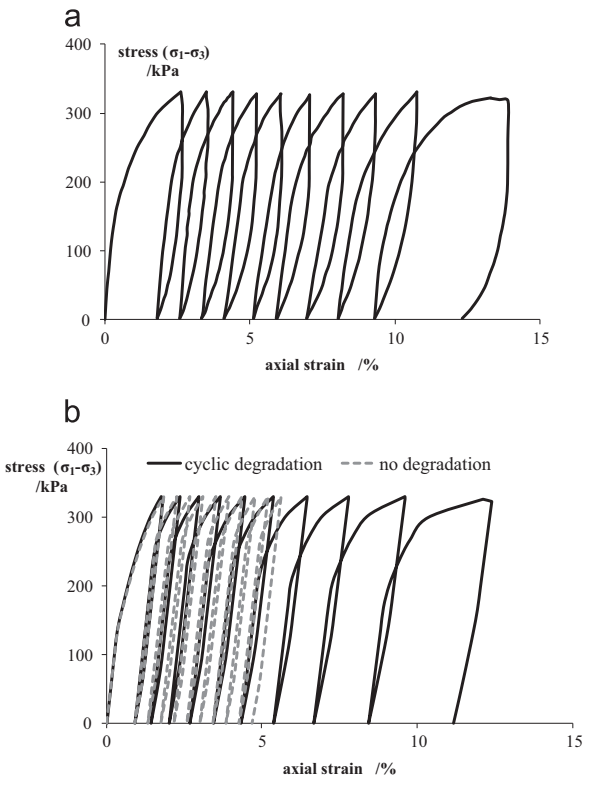

Fig. 6. Comparisons of stress–strain curves under one-way cyclic loading. (a) test result and (b) model prediction.

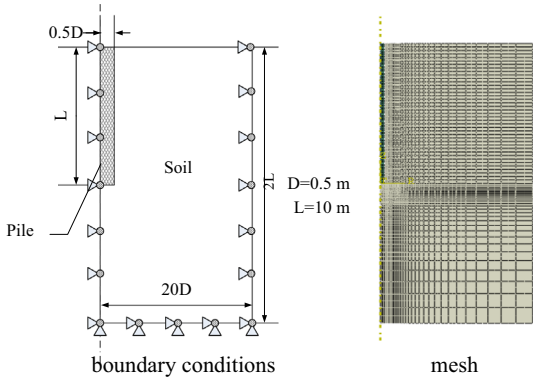

Fig. 7. Finite element model with a single pile.

Table 3
Parameters used in the finite element simulation of a single pile under cyclic loading.

Pile	Length L (m)	Diameter D (m)	Elastic modulus E (kPa)	Poisson's ratio ν			
	10	0.5	200,000	0.2			
Soil	Elastic modulus E (kPa)	Poisson's ratio ν	Plastic modulus C (kPa)	Initial yield stress A_0 (kPa)	Material parameter Q (kPa)	Nonlinear parameters γ	Damping factor b
	300	0.49	300	3.5	−3.5	22	1

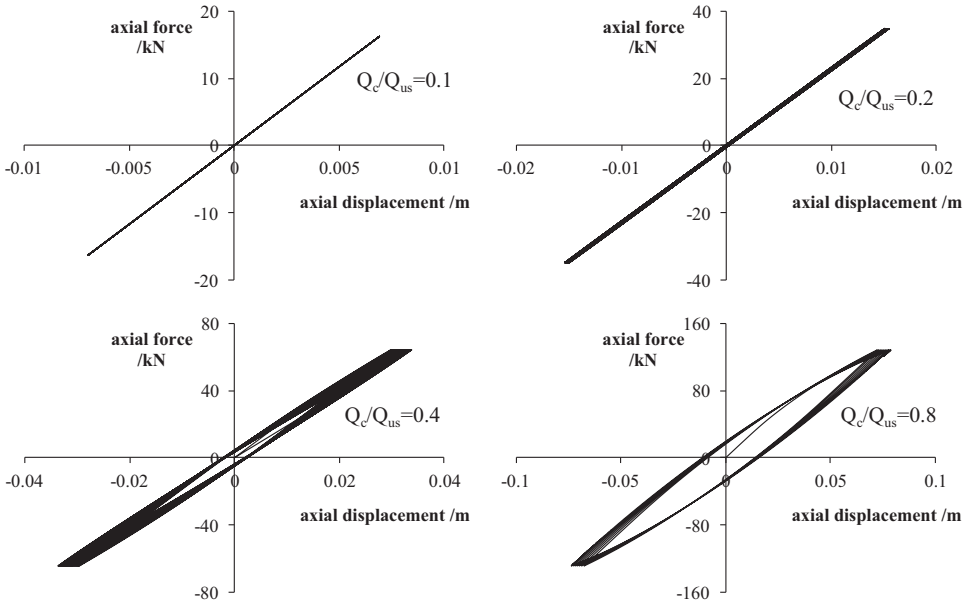

Fig. 8. Load–displacement curves of a single pile under axial cyclic loadings ($N=100$).

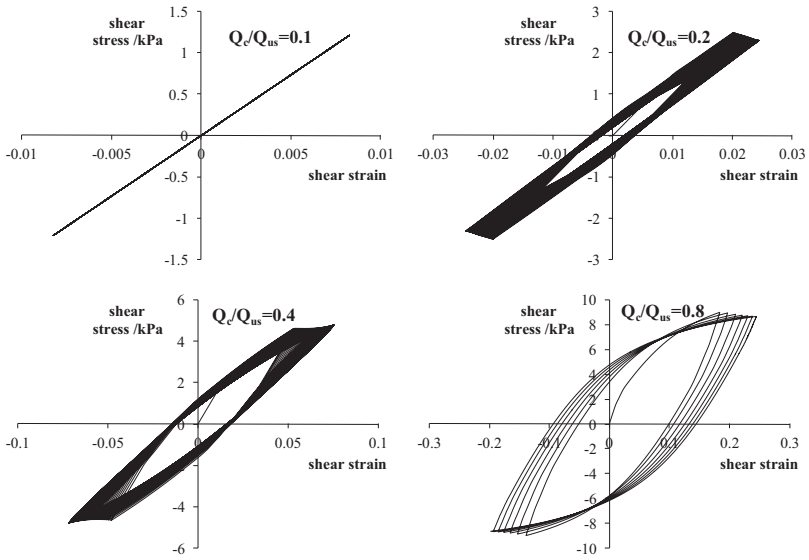

Fig. 9. Stress–strain curves of soil around pile top under cyclic loadings ($N=100$).

occurs. When the cyclic load level is big enough, degradation develops quickly. Under high levels of cyclic load, and when the cyclic shear stress at the pile side exceeds the residual strength ratio of the soil, failure occurs during cyclic loading. This explains, why no ultimate bearing capacity can be obtained when the cyclic load is bigger than 0.8.

3.2. Verification with experimental study (Poulos, 1979)

The experimental data of model piles provided by Poulos (1979) was used to further examine the efficiency of the finite element method based on the simplified kinematic hardening constitutive model. The tests were carried out on brass model piles with a diameter of 19 mm, an embedded length of 180 mm, and an elastic modulus E_p of 110,320 MPa, jacked into a bed of remoulded Darlington clay. The undrained strength of clay was 35 kPa kPa (Poulos, 1979), and the assumed value of elastic modulus was $E_s = 9$ MPa. The values of δ_{res} and b cannot be obtained directly from the results of the Poulos (1979) tests. However, in previous experimental studies (Sangrey et al., 1969; Andersen et al., 1980) it was reported that the undrained shear strength of clays after cyclic loading is rarely less than half of the initial undrained shear strength, and the degraded strength ratio was $\delta = 0.7 \sim 1.0$ in most cases. In the model tests, failure occurred at a cyclic load level $Q_c/Q_{us} = 0.56$ at the 64th cycle. Because the shear stress

level of the soil around the pile top is slightly higher than the cyclic load level at the pile top, the residual strength ratio δ_{res} was assumed to be 0.55, and the material parameter b was fixed at 1.0 after some adjustment.

After 100 times of cyclic load, the pile was loaded to failure at a constant rate of movement. The value of cyclic load level Q_c/Q_{us} was selected as 0.3, 0.4, 0.5, 0.55 and 0.6. Similar to the above section, a 2D axisymmetric model of this model test was set up. The load-displacement curves of model piles under cyclic and monotonic loading are shown in Fig. 11. The relatively good agreement between the numerical predictions and the experimental results achieved in the degraded ultimate bearing capacity after cyclic loading (Fig. 12) verifies that this FE analysis is both reasonable and reliable. The results from the test data and FE analysis indicate a similar trend in the degradation of the ultimate bearing capacity with the increase of cyclic load level, which develops slowly until the cyclic load level reaches a point where degradation develops rapidly within a small scope of cyclic load levels. However, because the degradation of the ultimate bearing capacity from the test data is dramatic at higher loading levels, it may well be that the estimated parameters are not accurate enough.

Although the simplified kinematic hardening model implemented in the finite element method can describe the cyclic degradation characteristic of axial pile foundation well, the computational load is huge. As such, this method is not suitable for calculating long-term cyclic loading. As a result, a more simplified analysis method for the axial capacity degradation of single piles under long-term cyclic loading is required for practical use in engineering applications.

4. A simplified analysis procedure for cyclic degradation of single piles

Due to the unsuitability of the FE analysis based on the kinematic hardening model considering cyclic degradation for calculating long-term cyclic loading, a more simplified analysis procedure based on a simplified nonlinear model is presented in the following section.

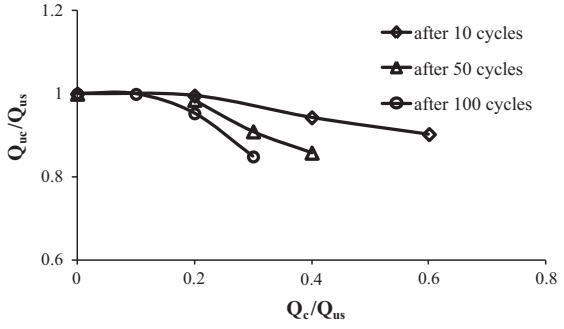

Fig. 10. Ultimate bearing capacity of single pile after cyclic loading.

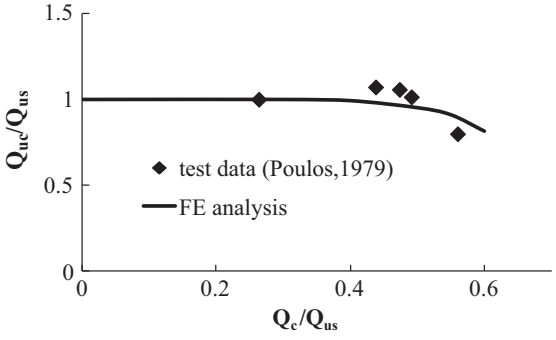

Fig. 12. Model validation against Poulos' model test.

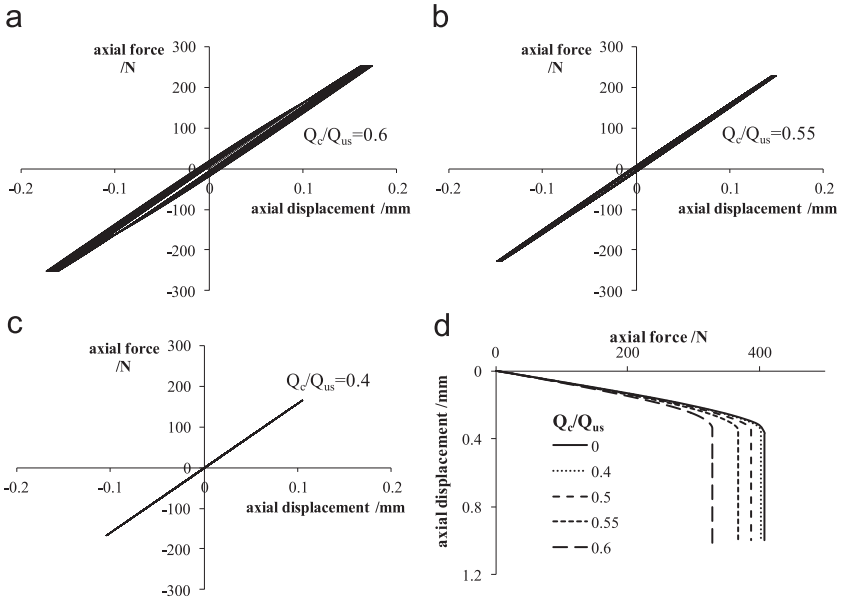

Fig. 11. Load–displacement curves of model piles under cyclic and monotonic loading. (a) cyclic loading, $Q_c/Q_{us}=0.6$, (b) cyclic loading, $Q_c/Q_{us}=0.55$, (c) $Q_c/Q_{us}=0.4$ and (d) monotonic loading after cyclic loading.

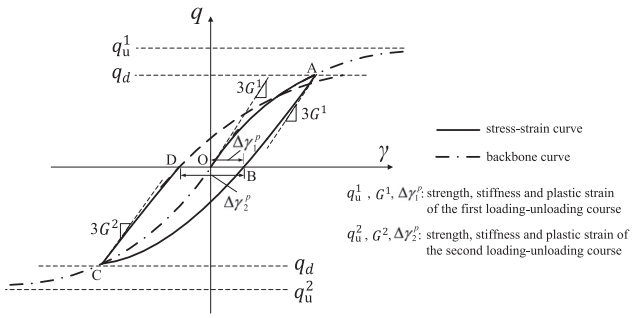

Fig. 13. Stress–strain hysteresis loops under cyclic loading with a amplitude of q_d.

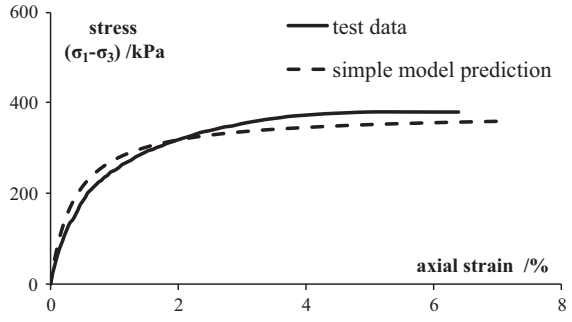

Fig. 14. Comparisons of stress–strain curves under monotonic loading.

4.1. A simple nonlinear model considering cyclic degradation

A simple nonlinear model considering cyclic degradation is presented to describe the stress–strain relations of clays under cyclic loading. This method is based on the pioneering work of Ramberg and Osgood (1943) and Hardin and Drnevich (1972). The stress–strain curves obtained during undrained cyclic loading consists of a series of cyclic loops composed of unloading and reloading branches. For convenience, the first cyclic loop of two-way cyclic loading with uniform amplitude of q_d is sketched in Fig. 13. The first loop contains the initial loading curve O–A, unloading curve A–B, reverse reloading B–C and reverse unloading C–D. q is the generalized shear stress, and γ is the generalized shear strain. For the triaxial condition, $q=\sigma_1-\sigma_3$ and $\gamma=(2/3)(\varepsilon_1-\varepsilon_3)$. For the pure shear condition, $q=\tau_{xy}$ and $\gamma=\gamma_{xy}$. In the case of undrained condition, i.e. $\varepsilon_v=0$, the equivalent strain ε_{eff} is identical to the generalized shear strain, i.e. $\varepsilon_{eff}=\gamma$.

The simple model can be expressed as

$$\gamma=\frac{q}{3G\left(1-(q/q_u)\right)} \tag{9a}$$

$$\gamma\pm\gamma_d=\frac{q\pm q_d}{3G}\left(1+\left|\frac{q\pm q_d}{\zeta q_u}\right|^n\right) \tag{9b}$$

in which G is the elastic shear modulus, q_d and γ_d are the stress and strain at the point of stress reversal, ζ and n are material parameters. n can control the shape of hysteresis loop. The larger the value of n, the thinner the hysteresis loops. The smaller the value of n, the fatter the hysteresis loops. ζ is the enlarged scale factor, reflecting the influence of loading mode. According to "Masing's Rule", the unloading stress–strain relationship keeps the same shape as that of the initial loading curve in the negative domain but is magnified by a factor of two, thus the enlarged scale factor $\zeta=2$ in two way cyclic loading. However, during one way cyclic loading, the shapes of and reloading curves are quite different from unloading curves, which have larger curvature, thus $\zeta=1$ was used for reloading while $\zeta=2$ was used for unloading. The value of the shape parameter n can be determined by fitting the test data.

In order to simulate strength and stiffness degradation due to undrained cyclic loading, Eqs. (9a) and (9b)) can be modified into

$$q_u=q_{u\,\max}+(q_{ures}-q_{u\,\max})(1-e^{-b\gamma^p}) \tag{10a}$$

and

$$G=G_0+(G_{res}-G_0)(1-e^{-b\gamma^p}) \tag{10b}$$

where $\gamma^p=\int\dot{\gamma}^p dt$ is the accumulative generalized shear strain, b has been defined in Eq. (6), G_0 is the initial elastic shear modulus and $G_{res}$is the final residual elastic shear modulus.

Eq. (9a) is adopted to describe the initial loading curve O–A, and Eq. (9b) is adopted to describe the subsequent stress–strain hysteresis loops. Take a cycle as an example (Fig. 13), these four curves can be divided into two loading–unloading courses, with corresponding unrecoverable plastic strains of $\Delta\gamma_1^p$ and $\Delta\gamma_2^p$. The strength and elastic shear modulus of the subsequent reloading–unloading course is degraded due

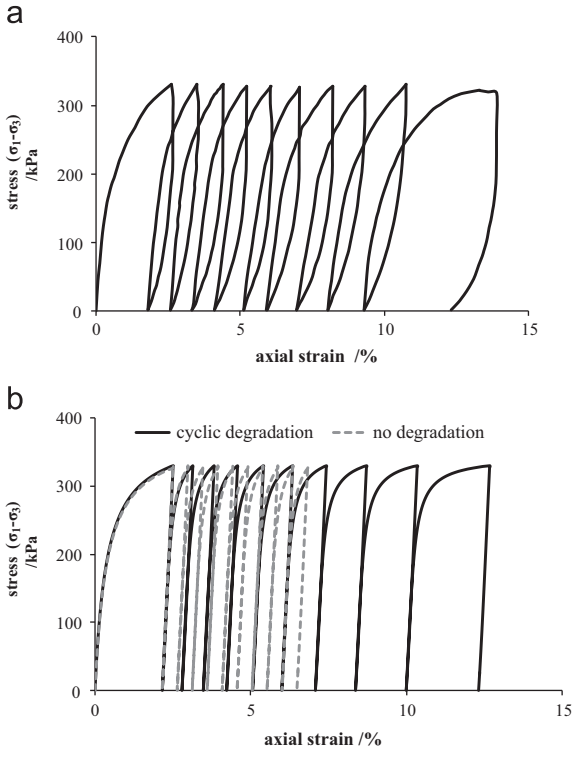

Fig. 15. Comparisons of stress–strain curves under one-way cyclic loading. (a) test result and (b) simple model prediction.

to the accumulative plastic strain γ^p ($\gamma^p = \sum \Delta\gamma_i^p, i = 1, 2, 3, 2N-1, 2N$).

The simple model was employed to simulate the experimental results of Sangrey et al. (1969). In the triaxial undrained condition, $\varepsilon_v^p = \varepsilon_1^p + \varepsilon_2^p + \varepsilon_3^p = 0$, considering $\gamma^p = (2/3)(\varepsilon_1^p - \varepsilon_3^p)$ and $\varepsilon_2^p = \varepsilon_3^p$, γ^p can be simply taken as ε_1^p. The enlarged scale factor $\zeta = 2$ was adopted for unloading and $\zeta = 1$ was adopted for reloading, with a shape parameter n is 3.6 after adjusting the parameters. Since there is an initial elastic stage in the kinematic hardening model, the initial tangent elastic modulus E in the simple model is much bigger than the elastic modulus in the kinematic hardening model, which was fixed at 100,000 kPa by adjusting parameter to the test results for monotonic loading. Other parameters were kept consistent with those in the kinematic hardening model. Figs. 14 and 15 show the comparisons of stress–strain curves predicted by the simple model with the test data under monotonic loading and cyclic loading. The good agreement obtained validates the efficiency of the simple model. The stress–strain hysteresis loops obtained from the simple model with no degradation considered are shown in Fig. 15(b). As was the case with the kinematic hardening model, the shape of the subsequent stress–strain hysteresis loops remains the same from the second loop. The convenience of this simple model for practical engineering applications was established by these comparisons.

4.2. A nonlinear shear displacement method based on the simple soil model

A simplified analysis procedure based on the shear displacement method for analyzing the behavior of single piles in clay under uniform cyclic axial loading is presented here in order to reduce the computational burden. The reduction of shaft stresses caused by cyclic loading is considered using the degradation of the elastic shear moduli and shaft limiting stress.

Fig. 16 shows a pile–soil system under two-way cyclic axial force loading with a constant amplitude p_0 at the pile top, with N representing the total number of cyclic loading. Because there are two loading–unloading courses in two-way cyclic loading, the total loading–unloading course number is $2N$. The soil parameters are assumed constant in the same loading–unloading course. The pile is divided equally into M elements to transfer the cyclic load from pile top to pile base. In the cyclic loading course i ($i = 1,2,\ldots,2N$), the amplitude of cyclic shear stress τ_j^i around pile element j ($j = 1, 2,\ldots,M$) can be calculated by obtaining the pile axial force through the shear displacement method (Cooke, 1974). The pile axial force can be obtained according to the previous reports (Randolph and Wroth, 1978; Mylonakis and Gazetas, 1998), in which the transfer matrix for single pile can be obtained by the method proposed by Mylonakis and Gazetas (1998). The main analysis procedures are outlined briefly in the following section.

Randolph and Wroth (1978) assumed that the soil surrounding the pile can be represented by distributed Winkler springs.

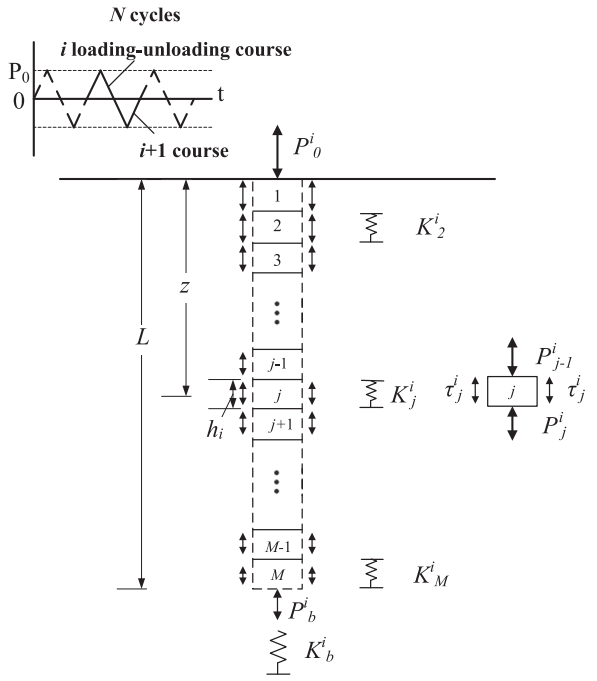

Fig. 16. Pile–soil system under two-way cyclic axial force loading.

The governing equation for pile–soil interaction is given below as

$$\frac{d^2 W_j^i(z)}{dz^2} - \left(\lambda_j^i\right)^2 W_j^i(z) = 0 \tag{11}$$

where $W_j^i(z)$ is the axial displacement of pile element j at cyclic loading course i. The variable λ_j^i is

$$\lambda_j^i = \sqrt{\frac{k_j^i}{A_p E_p}} \tag{12}$$

where E_p and A_p are Young's modulus and cross-sectional area of the equivalent solid cylinder pile, respectively. k_j^i is spring stiffness of the soil around the pile element j at cyclic loading course i,

$$k_j^i = \frac{2\pi}{\ln(r_m/r_0)} G_j^i \tag{13}$$

where G_j^i is the soil shear modulus around pile element j at cyclic loading course i, r_0 is the pile radius and r_m represents the maximum radius of influence of the pile beyond which the shear stress becomes negligible. $r_m = \chi_1\chi_2 L(1-\nu)$, $\chi_1\chi_2 \approx 2.5$ under the condition of homogeneous soil and $\chi_1\chi_2 \approx 1.0$ for Gibson soil (Mylonakis and Gazetas, 1998).

As to the stiffness of soil at the pile base K_b^i, it is reasonable to assume that the pile base acts as a rigid circular disk on the surface of a homogeneous elastic stratum (Randolph and Wroth, 1978).

$$K_b^i = \frac{P_b^i}{W_b^i} = \frac{dE_b^i}{1-\nu_b^2}\left(1 + 0.65\frac{d}{h_b}\right) \tag{14}$$

where E_b^i and ν_b are Young's modulus and Poisson's ratio of the soil at the pile base level, and d is the diameter of the pile.

P_b^i and W_b^i are the axial force and displacement at the pile base, and h_b is the depth of a rigid bedrock below the pile base.

The displacement along the pile $W_j^i(z)$ can be obtained by solving the differential Eq. (11),

$$W_j^i(z) = A_{11}\exp(\lambda z) + B_{11}\exp(-\lambda z) \tag{15}$$

where A_{11} and B_{11} are integration constants and can be obtained using the method proposed by Mylonakis and Gazetas (1998). For each soil layer, by imposing the continuity of forces and displacements at the interface, the relationship between the displacement and axial force at the pile base W_b^i and P_b^i and the displacement and axial force at the pile top W_0^i and P_0^i is

$$\begin{Bmatrix} W_b^i \\ P_b^i \end{Bmatrix} = [T^i] \begin{Bmatrix} W_0^i \\ P_0^i \end{Bmatrix} \tag{16}$$

where $[T^i] = \prod_{j=1}^{M} [t^i]_j$, the transfer matrices $[t^i]$ is

$$[t^i]_j = \begin{bmatrix} \cosh\left(\lambda_j^i h_j\right) & -E_p A_p \lambda_j^i \sinh\left(\lambda_j^i h_j\right) \\ -(E_p A_p \lambda_j^i)^{-1} \sinh\left(\lambda_j^i h_j\right) & \cosh\left(\lambda_j^i h_j\right) \end{bmatrix} \tag{17}$$

where h_j is the thickness of jth pile element.

Enforcing the boundary conditions $W_0^i = 1$ and $P_b^i = K_b^i W_b^i$, the stiffness of a single pile is easily obtained from Eq. (16),

$$K^i = \frac{K_b^i T_{11}^i - T_{21}^i}{T_{22}^i - K_b^i T_{12}^i} \tag{18}$$

For a given force atop the pile P_0^i, the pile response of any element j can be calculated as follows (Mylonakis and Gazetas, 1998):

$$\begin{Bmatrix} W_j^i \\ P_j^i \end{Bmatrix} = \prod_{k=1}^{j} [t^i]_k \begin{Bmatrix} \frac{1}{K^i} \\ 1 \end{Bmatrix} P_0^i \tag{19}$$

If the axial force of shaft element j is known, the amplitude of shear stress at pile–soil interface can be evaluated by

$$\tau_j^i = \frac{P_{j-1}^i - P_j^i}{U_p h_j} \tag{20}$$

When the shear stress at pile–soil interface τ_j^i reaches the limiting skin friction τ_{fj}^i, the soil around this element will enter into the plastic phase, and the excess load will transfer to the other element in elastic phase. In this condition, the transfer matrix is

$$\left[t_f^i\right]_j = \begin{bmatrix} 1 & -(E_p A_p \lambda_j^i)^{-1} h_j \\ 0 & 1 \end{bmatrix} \tag{21}$$

For the case of saturated clay foundation, the limiting skin friction τ_{fj}^i is equal to the undrained shear strength S_{uj}^i around the pile. For every element of the pile, once the cyclic axial force at the pile top is known, the cyclic shear stress of soil around the pile shaft elements can be determined (Eq. (20)). Then the soil plastic strain at every element can be obtained from the simple soil model (Eqs. (9) and (10)). The degraded ratio δ of strength and modulus of soil around the pile can be calculated by Eq. (6), thereby allowing the degraded strength and modulus to be obtained as well, and these renewed parameters are used in the next loading–unloading course. When the cyclic load level is sufficiently high, the axial force passed on to the pile base is large. This cannot be ignored, and the degradation of soil around pile base must be considered. The degraded moduli may be obtained similarly by

$$E_b^i = E_1^i[\delta_{res} + (1-\delta_{res})e^{-b\varepsilon_{eff}^{p,i}}] \tag{22}$$

where $\varepsilon_{eff}^{p,i}$ is the accumulated equivalent plastic strain of the soil around element M, and the degradation of the soil at the pile base is considered the same as the soil around element M.

The ultimate axial bearing capacity of pile is determined by utilizing the displacement–axial force curve of pile top, in which the axial force value of the turning point is defined as ultimate axial bearing capacity of the pile. Otherwise, in cyclic loading, failure occurs if the axial force of the pile base is bigger than the ultimate pile tip resistance (Skempton, 1951):

$$Q_{ult,b}^i = 9 S_{u,b}^i A_p \tag{23}$$

where $Q_{ult,b}^i$ is the ultimate pile tip resistance after ith loading–unloading course, and $S_{u,b}^i$ is the undrained shear strength of the soil at pile base after ith loading–unloading course.

4.3. Verifications of the simplified analysis method

The simple analysis method is verified against the results obtained from finite element method firstly. As the soil foundation is homogeneous, the value of $\chi_1\chi_2$ is set as 2.5, and the value of elastic modulus is set as 600 kPa though comparing with the calculated result of FEM. Other parameters keep track of those in FEM. The displacement–force curves obtained from FEM and the simple analysis method under static loading are shown in Fig. 17. The ultimate axial bearing capacity is the axial force value of the turning point in the displacement–axial force curve of the pile top. Compared to displacement–force curve of FEM, because the curve of the simple method is much smoother, the turning point is less obvious. These two curves intersect at the axial displacement of 0.15 m, thus the axial force of simple method corresponding to 0.15 m is identified as ultimate axial bearing capacity for future comparisons.

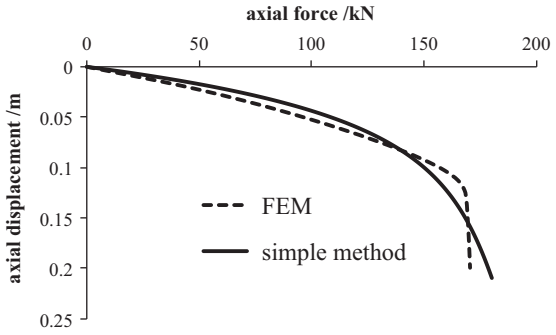

Fig. 17. Displacement–axial force curves of pile top under static loading.

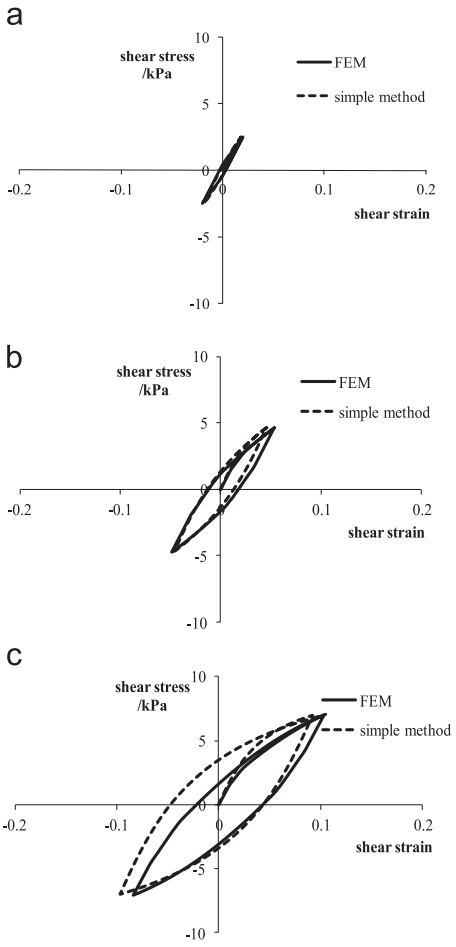

Fig. 18. Comparisons of stress–strain curves between the simple model and FEM at different Q_c/Q_{us}. (a) $Q_c/Q_{us}=0.2$, (b) $Q_c/Q_{us}=0.4$ and (c) $Q_c/Q_{us}=0.6$.

As this is two-way cyclic loading, the enlarged scale factor adopted was $\zeta=2$. In the absence of relevant tests data for the simple soil model, the shape parameter n is set as 1.5 by adjusting parameters to compare with stress–strain loops of the first cycle obtained from FEM at different cyclic load levels (Fig. 18). Although the shape of stress–strain loops obtained from these two methods are very close, discrepancies still exist. The stress–strain loops of simple method vary more significantly than that of FEM, e.g., the loop of simple method with current parameters is thinner than that of FEM at $Q_c/Q_{us}=0.4$ but fatter than that of FEM at $Q_c/Q_{us}=0.6$.

Comparisons of ultimate bearing capacities after different number of cycles and different cyclic load levels calculated by the two methods are shown in Fig. 19. The agreement is remarkably good, and the faster development of ultimate bearing capacity degradation at higher cyclic load levels is clear for both two methods. However, since there is no initial elastic stage in the simple nonlinear soil model, unlike the kinematic hardening model, cyclic degradation occurs at very low cyclic load levels. This discrepancy can be ignored when the number of cyclic loading is small. Theoretical results obtained from the simplified analysis procedure reveal similar valuable information about the effect of previous cyclic loading on the ultimate load capacity of single piles.

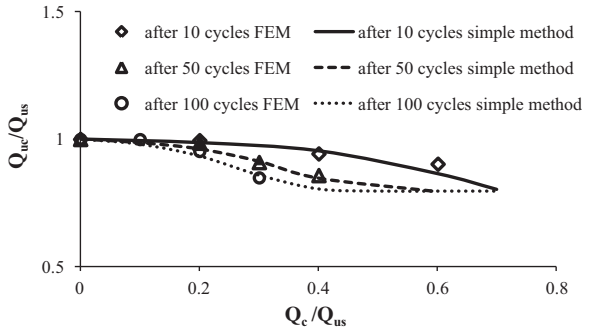

Fig. 19. The ultimate bearing capacity of single pile after cyclic loading (FEM and the simple method).

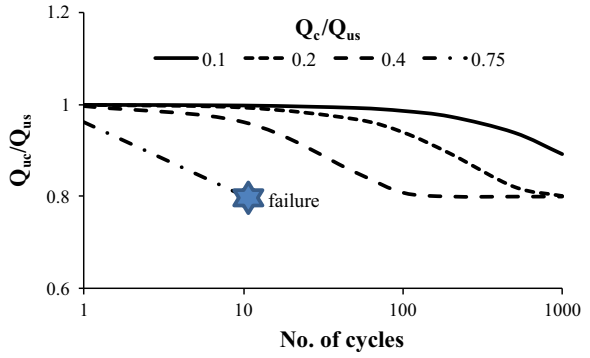

Fig. 20. The ultimate bearing capacity of single pile after long term cyclic loading by the simple method.

In addition to this, this method has the advantage of computational speed for long-term cyclic loading. The forecast of long term cyclic loading calculated by the simple method is shown in Fig. 20. Although the very little degradation occurred for low cyclic load levels after a few cycles ($Q_c/Q_{us}=0.1$, No. of cycles$=10$), the accumulative effect after long-term cyclic loading is obvious ($Q_c/Q_{us}=0.1$, No. of cycles$=1000$). It should be noted that this degradation was not clear in the results from FEM. A comparison of the curves of $Q_c/Q_{us}=0.2$ and $Q_c/Q_{us}=0.4$, the steady state of degradation will be achieved earlier at higher cyclic load level. Failure occurs after 11 cycles at $Q_c/Q_{us}=0.75$, which means at that time the cyclic shear stress at pile side has exceeded the residual strength ratio of the soil.

The simplified procedure was employed to simulate the model tests by Poulos (1979). The enlarged scale factor $\zeta=2$ was employed, as it was for two-way cyclic loading. In the absence of relevant test data for the simple soil model, the shape parameter n is set as 2.5 by comparing the first stress–strain loops with that in FEM (Fig. 21). The value of $\chi_1\chi_2$ is set as 1.1 and the elastic modulus is set as 12 MPa after referring to the static loading results calculated by FEM. The other parameters keep track of those in FEM. Good agreement between the simplified procedure and the experiment are also achieved in the degraded ultimate bearing capacity after a cyclic loading of $N=100$ and $N=1000$ (Fig. 22).

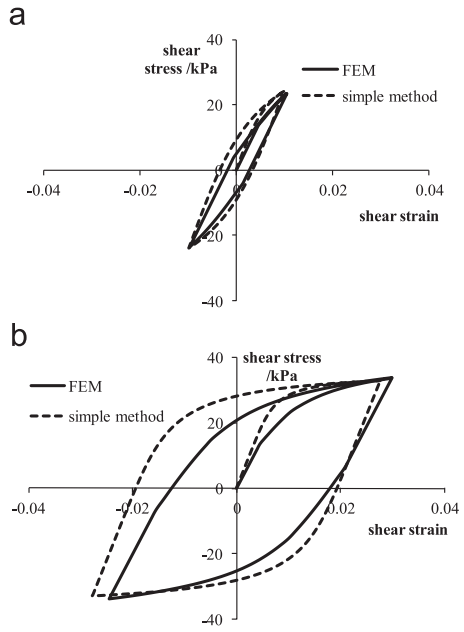

Fig. 21. Comparisons stress–strain curves of soil around pile top between of the simple model and FEM for Poulos' model tests. (a) $Q_c/Q_{us}=0.6$ and (b) $Q_c/Q_{us}=0.9$.

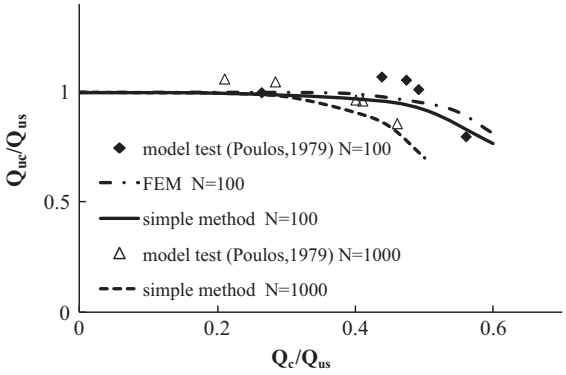

Fig. 22. The ultimate bearing capacity of single pile after cyclic loading (simple method, FEM and model test).

With fewer parameters and higher computational speed, the simple analysis method based on the simple soil model is a friendly engineering method for predicting the axial capacity degradation of single piles under long-term cyclic loading. However, the selection of the parameters is very important and any small deviation from true value is likely to result in significant error after a large number of load repetitions. Therefore, static and dynamic triaxial tests are needed to determine the soil parameters such as the shear modulus, undrained strength, shape parameter, and degraded parameters δ_{res} and b before engineering application.

5. Conclusions

A kinematic hardening constitutive model was developed for cyclic degradation to analyze the cyclic axial response of single piles in saturated clay using commercially available finite element software. A more simplified analytical approach based on a simple nonlinear model for cyclic degradation was suggested in order to reduce the computation burden. Both of these soil models were validated against dynamic triaxial test results (Sangrey et al., 1969), and both of these anaylsis methods were verified against the 1 g model tests by Poulos (1979).

- A cyclic degradation model for the strength of saturated clay was presented. This model is imported into the simplified kinematic hardening model provided in ABAQUS. Two modifications were made by user subroutine. The degradation of soil stiffness was complemented, and the size of the yield surface was set to remain unchanged under monotonic loading. This model was shown capable of predicting different behaviors of clay with increasing cyclic stress levels, including the elastic state, the elastoplastic steady state and the elastoplastic failure state. In the FEM based on the kinematic hardening model, the pile–soil system remains elastic without any degradation at low cyclic load levels. The ultimate axial bearing capacity of pile foundation degrades after cyclic loading, with degradation developing rapidly at higher cyclic load levels or after more loading cycles.
- In the simple nonlinear model, degradations for strength and stiffness of saturated clay were also considered. Because the simple model cannot describe the elastic stress–strain relations at low stress levels, discrepancies were apparent between cyclic degradations obtained from the FEM and the simple method at low cyclic load levels. Nevertheless, results calculated by this simple analysis at relatively high cyclic load levels were consistent with those of numerical simulation.

Unlike conventional theories which empirically express degradation factors as a function of the number of loading cycles, both the FEM and the simple method are based on the constitutive models of soil. This alone makes these models more consistent with theory and more reliable. Considering the complexity and diversity of soils, tests are necessary for geting exact parameters of the models. Still more research is in great need. The simple method has potential to serve as a useful tool in engineering design in the future.

Acknowledgement

This work was financially supported by the National Basic Program of China (973 Program, Grant no. 2013CB036304), the National Natural Science Foundation of China (Grant nos. 51378392 and 41362016). These supports are gratefully acknowledged.

References

Anastasopoulos, I., Gelagoti, F., Kourkoulis, R., et al., 2011. Simplified constitutive model for simulation of cyclic response of shallow

foundations: validation against laboratory tests. J. Geotech. Eng. ASCE 137, 1154–1168.
Andersen, K.H., Pool, J.H., Brown, S.F., et al., 1980. Cyclic and static laboratory tests on Drammen clay. J. Geotech. Eng. ASCE 106 (5), 499–529.
Armstrong, P.J., Frederick, C.O., A mathematical Representation of the Multiaxial Bauschinger Effect. CEGB Rep. No. RD/B/N 731, 1966.
Carter, J.P., Booker, J.R., Wroth, C.P., 1982. A critical state soil model for cyclic loading. In: Panda, G.N., Zienkiewicz, O.C. (Eds.), Soil Mechanics—Transient and Cyclic Loads. John Wiley & Sons Ltd., New York, pp. 219–252.
Cooke, R.W. The settlement of friction pile foundations. In: Proceedings of the Conference on Tall Buildings, Kuala Lumpur, Malaysia, 1974.
Giannakos, S., Gerolymos, N., Gazetas, G., 2012. Cyclic lateral response of piles in dry sand: finite element modeling and validation. Comput. Geotech. 44, 116–131.
Hardin, B.O., Drnevich, V.P., 1972. Shear modulus and damping in soils:design equations and curves. J. Soil Mech. Found. Eng. Div. ASCE 98 (7), 667–692.
Huang, M.S., Li, S., 2010. Degradation of stiffness and strength of offshore saturated soft clay under long-term cyclic loading. Chin. J. Geotech. Eng. 32 (10), 1491–1498 in Chinese.
Hyodo, M., Yamamoto, Y., Sugiyama, M., 1994. Undrained cyclic shear behavior of normally consolidated clay subjected to initial static shear stress. Soils Found. 34 (4), 1–11.
Jardine, R.J., Standing, J.R., 2012. Field axial cyclic loading experiments on piles driven in sand. Soils Found. 52 (4), 723–736.
Lee, C.Y., 1993. Cyclic response of axial loaded pile groups. J. Geotech. Eng. ASCE 119 (9), 1399–1412.
Lemaitre, J., Chaboche, J.L., 1990. Mechanics of Solid Materials. Cambridge University Press, Cambridge, UK.
Lombardi, D., Bhattacharya, S., Wood, D.M., 2013. Dynamic soil–structure interaction of monopole supported wind turbines in cohesive soil. Soil Dyn. Earthquake Eng. 49, 165–180.
Lesny, K., Hinz, P., 2009. Design of monopile foundations for offshore wind energy converters GSP No. 185. Contemp. Topics Deep Found. ASCE, 512–519.
Mróz, Z., Norris, V.A., Zienkiewicz, O.C., 1981. An anisotropic, critical state model for soils subject to cyclic loading. Géotechnique 31 (4), 451–469.
Mylonakis, G., Gazetas, G., 1998. Settlement and additional internal forces of grouped piles in layered soil. Geotechnique 48 (1), 55–72.
Poulos, H. G. ,Development of an analysis for cyclic axial loading of piles. In: Proceedings of Third International Conference on Numerical Methods in Geomechanics, Vol.4, Aachen, Germany, A. Balkema, Rotterdam, 1979, pp. 1513-1530.
Poulos, H.G., 1981. Cyclic axial response of single pile. J. Geotech. Eng. ASCE 107 (1), 41–58.
Poulos, H.G., 1987. Analysis of residual stress effects in piles. J. Geotech. Eng. ASCE 113 (3), 216–229.
Poulos, H.G., 1988. Cyclic stability diagram for axially loaded piles. J. Geotech. Eng. ASCE 114 (8), 877–895.
Prévost, J.H., 1977. Mathematical modeling of monotonic and cyclic undrained clay behavior. Int. J. Numer. Anal. Methods Geomech. 1, 195–216.
Ramberg, W., Osgood, W.R., 1943. Description of stress–strain curves by three parameters Technical Note 902. National Advisory Committee for Aeronautics, Washington, D.C.
Randolph, M.F., Wroth, C.P., 1978. Analysis of deformation of vertically loaded piles. J. Geotech. Eng. ASCE 104 (12), 1465–1488.
Sangrey, D.A., Henkel, D.J., Esrig, M.I., 1969. The effective stress response of a saturated clay soil to repeated loading. Can. Geotech. J. 6, 241–252.
Skempton, A.W., The bearing capacity of clays. In: Proceedings of Building Research Congress, vol. 1, 1951, pp. 180–189.
Soroush, A., Soltani-Jigheh, H., 2009. Pre- and post-cyclic behavior if mixed clayed soils. Can. Geotech. J. 46, 115–128.
Tsuha, C.H.C., Foray, P.Y., Jardine, R.J., et al., 2012. Behaviour of displacement piles in sand under cyclic axial loading. Soils Found. 52 (3), 393–410.
Zergoun, M., Vaid, Y.P., 1994. Effective stress response of clay to undrained cyclic loading. Can. Geotech. J. 31, 714–727.